Identifying and Mitigating the Effects of Air Gaps in Material Characterization Using Terahertz Time-Domain Reflection Spectroscopy

Preprint · December 2024

DOI: 10.13140/RG.2.2.28342.00322

4 authors, including:

Juin W. Zhou
Stony Brook University
22 PUBLICATIONS **148** CITATIONS
SEE PROFILE

Omar Bassam Osman
30 PUBLICATIONS **367** CITATIONS
SEE PROFILE

M. Hassan Arbab
Stony Brook University
91 PUBLICATIONS **969** CITATIONS
SEE PROFILE

Identifying and Mitigating the Effects of Air Gaps in Material Characterization Using Terahertz Time-Domain Reflection Spectroscopy

JUIN W. ZHOU, ZACHERY B. HARRIS, OMAR B. OSMAN AND M. HASSAN ARBAB*

Department of Biomedical Engineering, Stony Brook University, Stony Brook, NY 11790 USA
**hassan.arbab@stonybrook.edu*

Abstract: Terahertz time-domain spectroscopy (THz-TDS) in reflection mode is a powerful technique for extracting the broadband dielectric function of materials in many applications. However, it is very sensitive to the phase ambiguity problem due to any misalignment between the sample and reference positions. Several computational methods have been developed over the years to address this limitation. One solution to the phase ambiguity problem is the use of imaging windows, which allows for a self-referenced measurement strategy. However, this method can give rise to the presence of air gaps between the sample and window, and introduce other sources of measurement error. The trapped air gaps can occur inevitably, and are difficult to identify, in complex targets, such as those with rough surfaces or sub-wavelength air voids. In this paper, we present a novel method for identifying such air gaps, estimating their size, and computationally removing the resultant artifacts in spectroscopic measurements. Our approach is based on modeling the complex index of refraction of the sample in the presence of an air gap and extracting its thickness using the so-called quasi-space approach. We verify this technique in the analysis of *in vivo* THz images of skin tissue and using controlled test samples composed of a multi-layer structure of an air gap trapped between an imaging window and an HDPE pellet. In both cases, we show that the proposed method can extract the thickness of the air gap and calculate the refractive index of the sample accurately.

1. Introduction

Terahertz time-domain spectroscopy (THz-TDS) has found many applications in studying new material properties, exploring ultrafast phenomena, biomedical sensing and imaging, and quality control in industrial manufacturing [1]. One of the attractive features of the THz-TDS method is its ability to extract the broadband complex dielectric function of a sample from a single measurement [2]. It can be implemented in different experimental geometries, such as the transmission or reflection modes, among several other optical configurations. However, the reflection mode is often the only viable geometry in many applications, where the sample is highly attenuating or semi-infinite, examples of which include biomedical imaging [3–11], chemical and molecular analysis [12, 13], standoff detection of chemicals [14, 15], illicit drugs [16], and other harmful substances [17].

Despite its utility and versatility, the THz-TDS technique in the reflection geometry is highly sensitive to the phase ambiguity artifacts, in which a small displacement between the reference and sample positions introduces a phase shift and alters the complex spectral data [18]. A few solutions to this problem have been proposed. In spectroscopic methods, where a reflection from a mirror is used as the reference measurement, this problem has been addressed by subtracting the slope of the phase function [18] or using custom sample geometries such as a step-edge over a substrate [19] to remove the displacement error. However, because these methods assume either a linearly-dependent phase shift or a uniform sample thickness, their utility is limited

and not suitable for many diverse applications, where sample surface properties cannot be controlled. An alternative solution for obtaining reference measurements, which is uniquely suitable for biomedical applications, is to place an optically transparent window on the sample. This method provides two choices of reference at either the air-window (first) interface [20, 21] or the window-air (second) interface [3]. Regardless of the choice of the interface, they can effectively remove this phase error, and are independent of the sample thickness. However, using an imaging window can introduce new sources of measurement error because this approach assumes that there is a perfect contact between the sample and window. It is not always possible or practical to achieve a perfect surface contact. For example, air gaps may appear between the window and sample due to user error or the sample's surface properties [3, 22]. Moreover, applying pressure to the sample may remedy these air voids, but it may also produce new effects, such as occlusion in biological samples [23]. The existence of such errors due to voids, air gaps or occlusion affects are not easy to detect, particularly in heterogeneous samples. Finally, air gaps can occur naturally in some non-destructive testing applications such as identification of delamination between sample layers. Therefore, a computational strategy that can detect the presence of air gaps and remove any spectroscopic artifacts in the characterization of the sample properties are very useful in these applications.

In this paper, we present a THz-TDS computational approach that identifies the existence of an air gap and subsequently minimizes its impact on measurements by solving for its thickness and extracting the accurate complex index of refraction of the materials. Our technique draws inspiration from material characterization methods used in transmission geometry [24–26]. These methods simultaneously extract the thickness and refractive index of the sample. Assuming an air gap is always present in the sample, we derive a transfer function that models the propagation of the THz pulse through an imaging window and an air gap of unknown thickness d_a, and reflecting off a sample with index of refraction $\tilde{n}_s$, which is to be extracted by the model. By varying the thickness of the assumed air gap, we calculate a corresponding $\tilde{n}_s$, and then select the correct thickness and index of refraction based on a modification of the so-called "quasi-space" technique [25]. The paper is organized as follows. First, we will discuss the inefficiencies of the current computational methods for extraction of the sample's complex index of refraction, and derive a new transfer function in the presence of air gaps. Next, we will demonstrate the extraction of the air gap thickness in the time-domain and the refractive index of the sample in the frequency-domain. Finally, we will propose an alternative method of simultaneously extracting both thickness and refractive index in the frequency-domain. We will show using both *in vivo* skin measurements and manufactured samples with known physical properties that our proposed algorithms can detect the presence of very small air gaps, estimate its thickness, and accurately extract the index of refraction of a sample.

2. Theory

Figure 1 shows the transmitted and reflected beams by comparing the case for an ideal contact between the spectroscopy window and sample (left) to the case where an air gap is present at this interface (right). Existing models usually consider the ideal contact case, whereas in many biomedical tissue imaging and industrial applications with rough-surface or non-uniform samples [27–29] the presence of a trapped air gap between the sample and window can give rise to multiple internal reflection beams, shown for example by the multiple reflection arrows in Fig. 1. The complex reflectivity response of the sample system to the THz pulse can be modeled by the Fresnel transmission, reflection, and the propagation coefficients. At normal incidence angle, these coefficients are given by,

$$t_{01}(\omega) = \frac{2\tilde{n_0}(\omega)}{\tilde{n_0} + \tilde{n_1}}, \tag{1}$$

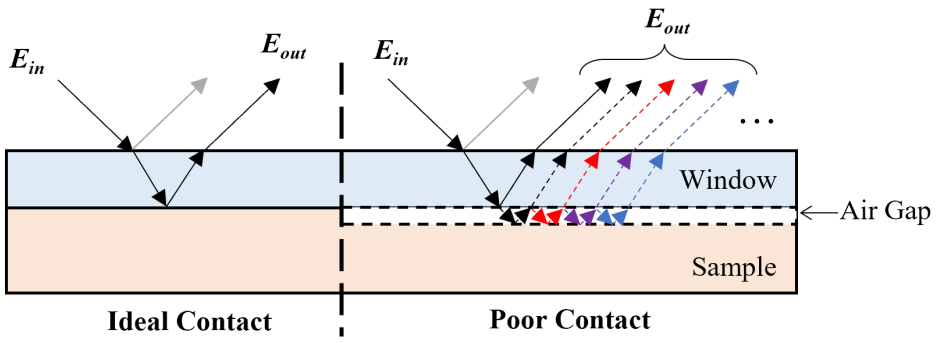

Fig. 1. The ideal contact produces a reflected THz pulse that is purely from the window-sample interface. This signal allows for direct calculation of the complex index of refraction of the sample, $\tilde{n}(\omega)$. In contrast, a sample measurement containing an air gap produces a reflected signal that contains the multiple reflections between the window and sample. For thin air gaps, the pulses from these echoes are superimposed, and cannot be separated easily if the thickness of the air gap is small, as compared to the THz pulse width.

$$r_{01}(\omega) = \frac{\tilde{n_0}(\omega) - \tilde{n_1}}{\tilde{n_0} + \tilde{n_1},}, \tag{2}$$

and

$$p_0(\omega) = \exp\left(-\frac{j\tilde{n_0}(\omega)d_0\omega}{c}\right), \tag{3}$$

where t_{01} is the transmission coefficient from medium 0 through medium 1 (henceforth, the "01 interface"), r_{01} is the reflection coefficient at the 01 interface, p_0 is the propagation through medium 0, d_0 is the propagation distance of the THz beam through medium 0, c is the speed of light, and ω is the angular frequency in which $\omega = 2\pi f$. The eventual transfer function depends on the choice of the reference measurement [3, 21]. The model presented in this paper uses the pulse reflected from the second window-air interface (without the presence of the sample), as the reference measurement. Therefore, all associated baseline removal and calibration methods described in Ref. [30] will also be applied in our signal processing steps.

The pulse reflected from the window-air interface, i.e, E_{ref}, can be modeled by,

$$E_{ref} = p_a^2 t_{aw} r_{wa} t_{wa} p_w^2, \tag{4}$$

where the subscripts "ref", a, and w represent reference, air, and window, respectively. Also, the pulse reflected from a sample in an ideal contact with the window can be described similarly as,

$$E_{samp,ideal} = p_a^2 t_{aw} r_{ws} t_{wa} p_w^2, \tag{5}$$

where the subscripts s refers to sample surface and "$samp, ideal$" refers to the sample measurement with ideal contact. The transfer function, $H(\omega)$, describes the sample's response to the THz beam, and can be calculated by dividing the sample reflection measurement in this geometry by the reference,

$$H(\omega) = \frac{E_{samp}}{E_{ref}}, \tag{6}$$

and modeled by,

$$H_{ideal}(\omega) = \frac{E_{samp,ideal}}{E_{ref}} = \frac{r_{ws}}{r_{wa}}. \tag{7}$$

Equation 7 is not dependent on the thickness of the spectroscopy window and allows for direct calculation of $\tilde{n}_{samp}$ using Eq.2, as given by the relationship,

$$\tilde{n}_s = \frac{\tilde{n}_w(\omega)(1 - H(\omega)r_{wa})}{1 + H(\omega)r_{wa}}. \tag{8}$$

However, in the presence of an air gap, the THz beam's path to the sample must include the propagation through the air gap. Therefore, when an air gap is present, the sample measurement with a single internal reflection can be modeled as,

$$E_{samp,gap} = p_a^2 t_{aw} p_w^2 t_{wa} \left(r_{wa} + t_{wa} p_{gap}^2 r_{as} t_{aw} \right). \tag{9}$$

Here, we assume that the amplitude of the subsequent reflection echos inside the spectroscopy window or the air gap are negligible. Thus, the transfer function for a sample in the presence of an air gap, $H_{gap}(\omega)$, can be simplified by,

$$H_{samp,gap}(\omega) = 1 + \frac{p_{gap}^2 r_{as} t_{aw} t_{wa}}{r_{wa}}. \tag{10}$$

Eq. 10 depends on the index of refraction of the sample, given by $\tilde{n}_{samp} = n - ik$, as well as the thickness of the air gap, defined by d_a, through the p_{gap}^2 term. However, in contrast to Eq. 7, which can be used to directly calculate n, and k from the measured values, here there is no comparable solution for Eq. 10. In other words, the values of the desired unknowns n, k, and d_a can not be solved directly. Therefore, an assumption must be made about either the thickness of the air gap or the index of refraction of the sample. In the following two sections, we will present two optimization techniques for extraction of these material parameters. The first technique uses a fixed index of refraction and extracts the thickness of the air gap in the time-domain. The second method fixes the thickness of the air gap within a range of estimated thicknesses, and solves for a unique index of refraction corresponding to that thickness. This method can therefore simultaneously extract the thickness of the air gap and index of refraction of the sample.

3. Time- and frequency-domain extraction of both thickness and complex index of refraction

3.1. Experimental methods for imaging burned skin

In this section, we will present skin imaging data collected in an *in vivo* porcine study. The experimental animal protocol was reviewed and approved by the Institutional Animal Care and Use Committee at Stony Brook University. The animal preparation, and tissue models are discussed in detail in Ref. [31, 32]. The particular burn wound investigated in this paper was created using a contact device heated to 80°C and placed onto the skin for 10 seconds. The burn wound was imaged using our custom handheld terahertz imaging device, the PHASR Scanner, which is further detailed in Ref. [33]. In this device, the sample remains in place while the THz beam is scanned across the window and reflected at normal incidence using a telecentric beam steering approach and an f-θ objective lens.

3.2. Data analysis and signal processing

THz-TDS images obtained using the PHASR Scanner consist of a 27x27 grid of 1 mm pixels, where a complete time-domain waveform is captured at each pixel. Each THz-TDS waveform measurement with an imaging window produces two THz pulses: a pulse corresponding to the

reflection from the air-window interface and another signal due to the window-sample interface. In addition to images of the sample, a reference (air) and baseline (water) measurement are also captured. The THz signal was processed using the baseline correction algorithm described in Ref. [30]. The refractive indices of the sample were extracted using the ideal-contact transfer function proposed in Ref. [3]. Figure 2(a) and (b) show a photo of an example burned skin and the corresponding THz images generated by the average real part of the index of refraction between 0.2 and 0.6 THz at each pixel. Pixels in which the average index of refraction was non-physical (i.e., $n < 1$, or $k > 0$) were set to 0 and appear black in Fig. 2b. The white region of interest (ROI) outlines the area of the sample in which the burn is in ideal contact with the imaging window. Due to the homogeneity of this representative burn and the surrounding pixels, we assume that the index of refraction was consistent throughout the entire wound [34]. Figure 2(c) and (d) show the real and imaginary part of the index of refraction extracted from the THz-TDS measurements shown in the red and white ROIs in Fig. 2b. It is evident that when the imaging window is in ideal contact with the tissue, the n and k values are realistic, whereas in the presence of an air gap, non-physical values can be extracted if the existence of this gap is not included in the model.

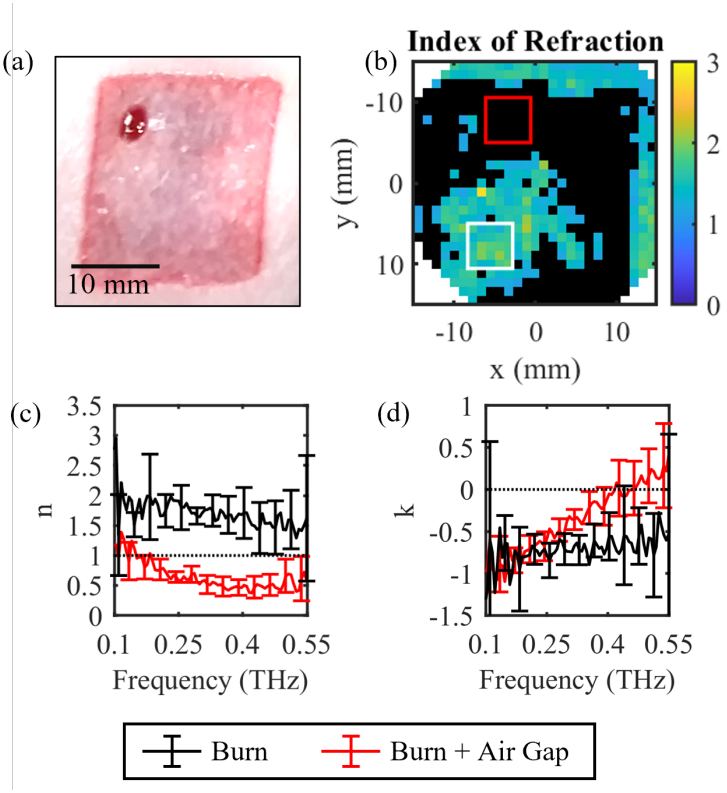

Fig. 2. (a) A sample of burned porcine skin was imaged using our custom handheld scanner. The tissue is debrided (i.e., the epidermis is removed from the damaged tissue), which creates a step from the healthy skin to the burned tissue. (b) The average index of refraction between 0.2 – 0.6 THz in the corresponding THz image. Using current methods, the index of refraction of the red ROI are non-physical as shown in (c) and (d). Pixels with non-physical values of n were set to black (about 57.02% of the image).

Next, we used the spatially averaged index of refraction of the white ROI and the reference measurement at each pixel to simulate the time-domain signal of a burn with and without an air gap. We compared the simulated pulses to the corresponding measured time-domain waveforms,

and extracted the thickness of an assumed air gap layer by minimizing the difference between the theoretical and measured pulses. This analysis results in a map of the air gap thickness of the sample measurement, which will be presented in the next section of this paper.

To extract the index of refraction of the red ROI (in the presence of the air gap), we used the thickness map calculated in the previous step in the frequency-dependent transfer function derived earlier, Eq. 10. We extract the index of refraction by minimizing the error between the calculated and measured transfer function, $\hat{H}(\omega)$ and $H_{samp}(\omega)$, respectively. The error function, H_{err} is defined by combining the difference of the magnitude and phase of the theoretical and measured transfer function, $\Delta|H(\omega)|$ and $\Delta\angle H(\omega)$, respectively [24]. These terms are defined by,

$$\Delta|H| = |H_{samp}(\omega)| - |\hat{H}(\omega)|, \tag{11}$$

$$\Delta\angle H = \angle H_{samp}(\omega) - \angle\hat{H}(\omega), \tag{12}$$

and

$$H_{err} = \sqrt{\Delta|H(\omega)|^2 + \Delta\angle H(\omega)^2}. \tag{13}$$

3.3. *Results obtained using burned skin samples*

Fig. 3a shows the comparison between the THz-TDS pulses reflected from the sample with an ideal contact with the imaging window (dotted blue line) and the measured pulse in the presence of an air gap (solid black line). By optimizing the thickness of the assumed air gap, as shown in Fig. 3b, this value is found to be 111 μm at the center of the red ROI in the burned tissue. A map of the extracted air gap thickness at each pixel is shown in Fig. 3c. It can be seen that the air gap is not uniform throughout the sample, and the average extracted thickness of the selected red ROI is 126.5 μm. The thickness of the air gap increases moving away from the center of the burn. The average extracted thickness is in accordance with the expected depth of the epidermis of porcine skin, which was removed during burn debridement.

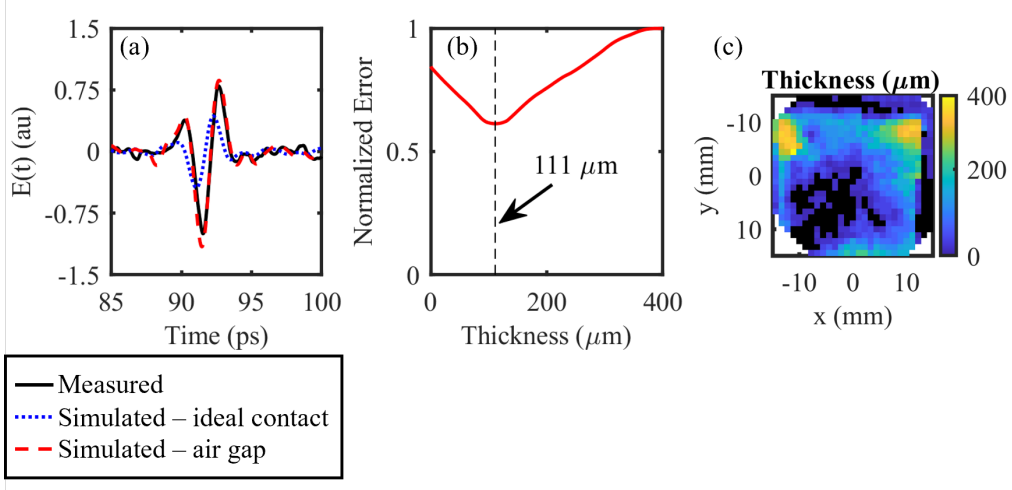

Fig. 3. (a) The measured TDS signal (black) is compared to the theoretical ideal contact scenario (blue, dotted) and the simulation of reflection in the presence of an air gap (red, dashed). The air gap thickness was varied between 0 and 400 μm. (b) The normalized error between the measured and simulated signals was minimized at 111 μm in this representative pixel (center of the red ROI). (c) map of the extracted air gap thicknesses.

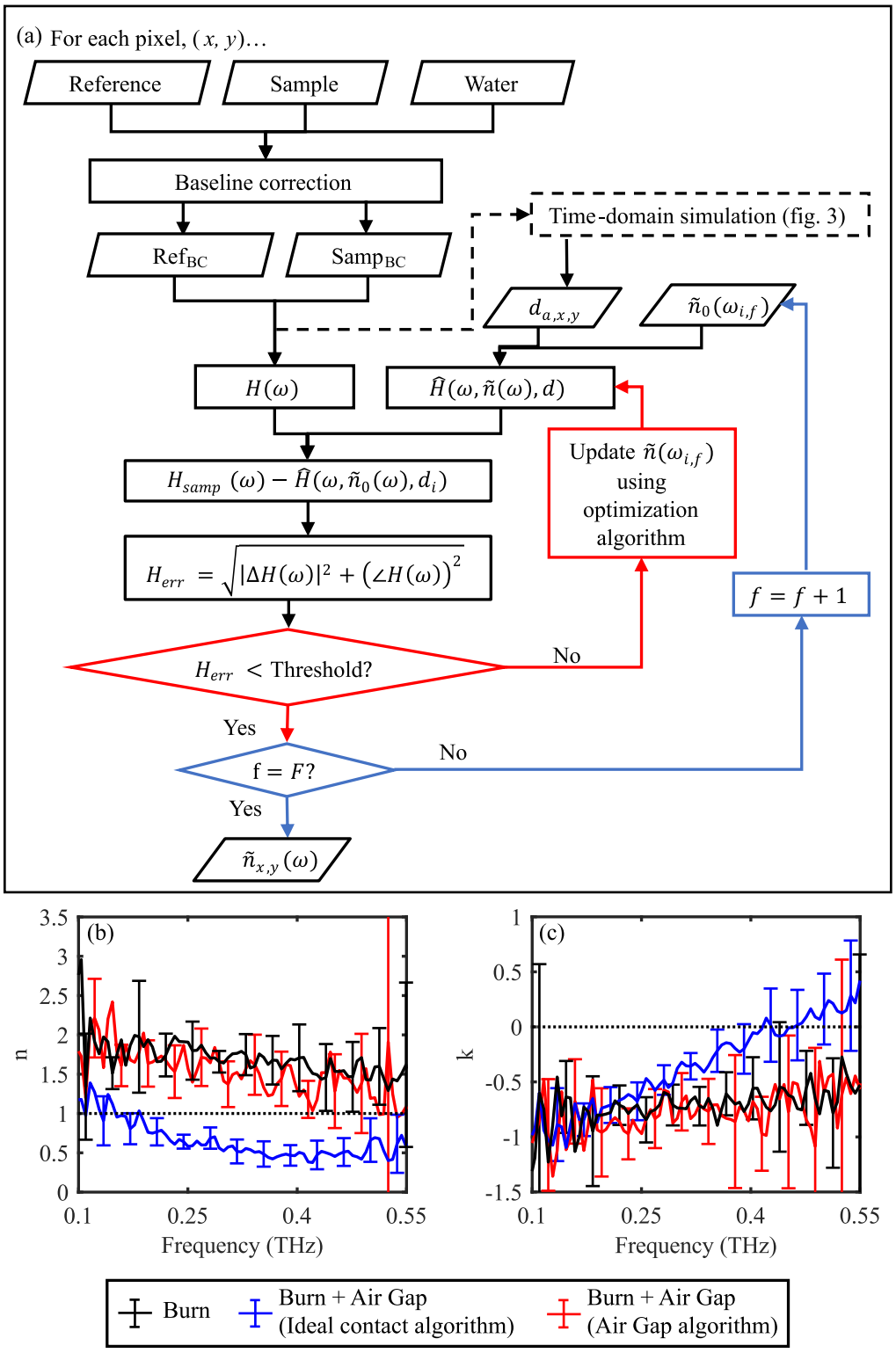

Fig. 4. (a) The flow chart details the steps of extracting the index of refraction of the red ROI of Fig. 2. The thickness extracted from the time-domain simulation is used to directly calculate the index of refraction. The real (b) and imaginary (c) parts of the index of refraction are shown. Compared to the ideal contact model (blue line) that yields non-physical values, the proposed algorithm (red) extracts the accurate index of refraction in the presence of air gap, which is in agreement with similar results obtained over ROIs without such gaps (black).

Fig. 4a shows the flow chart used in this section. At each pixel of the image, after the preliminary signal processing steps described earlier, the thickness of the assumed air gap, d_a, is optimized until the difference between the modeled and experimental transfer functions, i.e., H_{err}, is minimized. The initial value of the complex index of refraction of the tissue, $n_0(\omega)$, is assumed using double Debye dielectric function for healthy skin. The index of refraction produced from the ideal-contact and air gap models are compared in Fig. 4b-c. The ideal-contact function produces non-physical values of $n < 1$ for the red ROI in Fig. 2b. In contrast, the values extracted by the proposed air gap model after the optimization in this flowchart are nearly identical to the expected value of the ideal contact scenario.

4. Simultaneous extraction of air gap thickness and complex index of refraction in the frequency-domain

4.1. Experimental and signal processing methods

4.1.1. Simulation of a fabricated sample with known air gap thickness

To develop an algorithm to extract the air gap thickness, we simulated a THz-TDS measurement from a multi-layer sample composed of a HDPE pellet, a 280 μm air gap and an imaging window, as shown in Fig. 5a. Using Eq. 10, we assumed different guess for the thickness of the air gap layer, and extracted the index of refraction at each guessed value, d_i. The simulation results, shown in Fig. 5 (b) and (c), demonstrates that as d_i deviates from the correct thickness, d_a, both the real and imaginary parts of the index of refraction change in phase. This observation contrasts with transmission measurements, in which the *amplitude* of the Fabry-Perot oscillations increases [24, 25]. In transmission spectroscopy, to extract the thickness of a layer, the Fourier transform of the predicted refractive indices as a function of frequency was calculated, and the peak of the amplitude in the "quasi-space" domain was minimized [25]. We adopt this quasi-space analysis for reflection measurements. However, rather than analyzing the magnitude, we examine unwrapped phase in the quasi-space domain. The simulation reveals that the unwrapped phase of the correct thickness value is bound between -π to π. Additionally, the correct thickness produces the highest oscillatory amplitude in the quasi-space domain, as demonstrated in Fig. 5d.

4.1.2. Measurements of the fabricated sample

To experimentally validate the simulation, we placed a 4 mm thick HDPE pellet in a custom-made cuvette. A New York City transportation pass card (Metropolitan Transportation Authority, New York, NY, USA) is used to create the spacer. The thickness of the card was measured with a caliper to be 280 μm.

The measurement set-up has previously been described in Ref. [12]. Note, the table-top system for this experiment is distinct from the aforementioned PHASR Scanner. In brief, this bench-top system uses a commercially-available THz spectrometer (TeraSmart, Menlo Systems GmbH, Martinsried, Germany). We aligned the system in reflection mode at normal incidence to the sample. The cuvette is mounted onto a motorized stage (Newport Corporation, Irvine, CA, USA) and is scanned across the THz beam. A row of 10, 2 mm^2 pixels are measured; each pixel consists of 1000 time averages.

4.1.3. Data Analysis and Signal Processing

The THz measurements were prepared using the same signal processing methods described in section 3.2. Each thickness guess, d_i, results in a unique refractive index, $\tilde{n}_i(\omega)$, such that $H_{samp}(\omega) = \hat{H}(\omega, \tilde{n}_i(\omega), d_i)$. A Fourier transform is applied to $n_i(\omega)$ between 0.2 - 1 THz. We used the criteria revealed by the simulations in the previous section to extract the correct air gap thickness and the resulting index of refraction. This procedure was repeated for all pixels. This algorithm is summarized in Fig. 6.

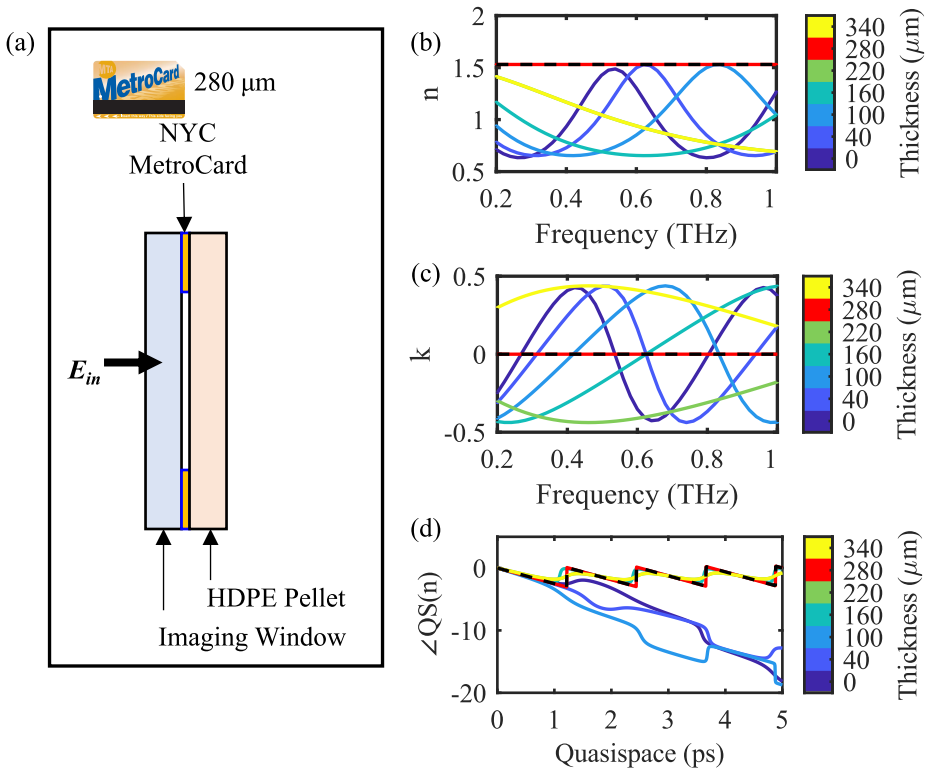

Fig. 5. (a) An air gap is created by placing a 280 μm spacer between an imaging window and HDPE pellet. This sample measurement was simulated and the (b) real and (c) imaginary parts of the index of refraction were extracted at different thickness guesses. At incorrect thicknesses, the simulation reveals that the amplitude of the index of refraction remains the same and the frequency of oscillations increases with increasing Δd. (d) The Fourier transform on the real index of refraction as a function of frequency reveals that the correct thickness produces an oscillatory phase function with phase confined between -π to π and the highest amplitude (red color in agreement with the correct thickness in black).

4.2. Results obtained using fabricated test sample

The results of the quasi-space domain analysis are presented in Fig. 7. Fig. 7(a) and (b) illustrate $n(\omega)$ and $k(\omega)$ extracted from both the ideal contact calculation and air gap algorithm.

At $d_i = 0$ μm, both the real and imaginary parts of $\tilde{n}(\omega)$ (blue lines) exhibit a large oscillatory behavior and deviates from the expected value,i.e., $\tilde{n}(\omega) = 1.53$. In contrast, the average extracted thickness (red line) illustrate a reduced variation effect and more closely resembles the known values of the complex index of refraction. Although the average $n(\omega)$ deviates from the expected value, the mean extracted $k(\omega)$ is exactly in agreement with the expected value. This effect is an artifact from the baseline correction, in which the $n(\omega)$ is offset from the expected value while $k(\omega)$ is accurately extracted [30].

Fig. 7c illustrates the unwrapped phase in the quasi-space domain for $d_i = 0\mu$m (ideal contact), $d_i = 280\mu$m (expected), and $d_i = 325\mu$m (extracted) for a single pixel. For $d_i = 0\mu$m and $d_i = 280\mu$m, the unwrapped phase exceeds the boundaries previously determined by the simulation. The extracted value, $d = 325\mu$m fulfills the specifications, such that the unwrapped phase is bound from -π to π, and exhibits the largest amplitude. The extracted thickness values

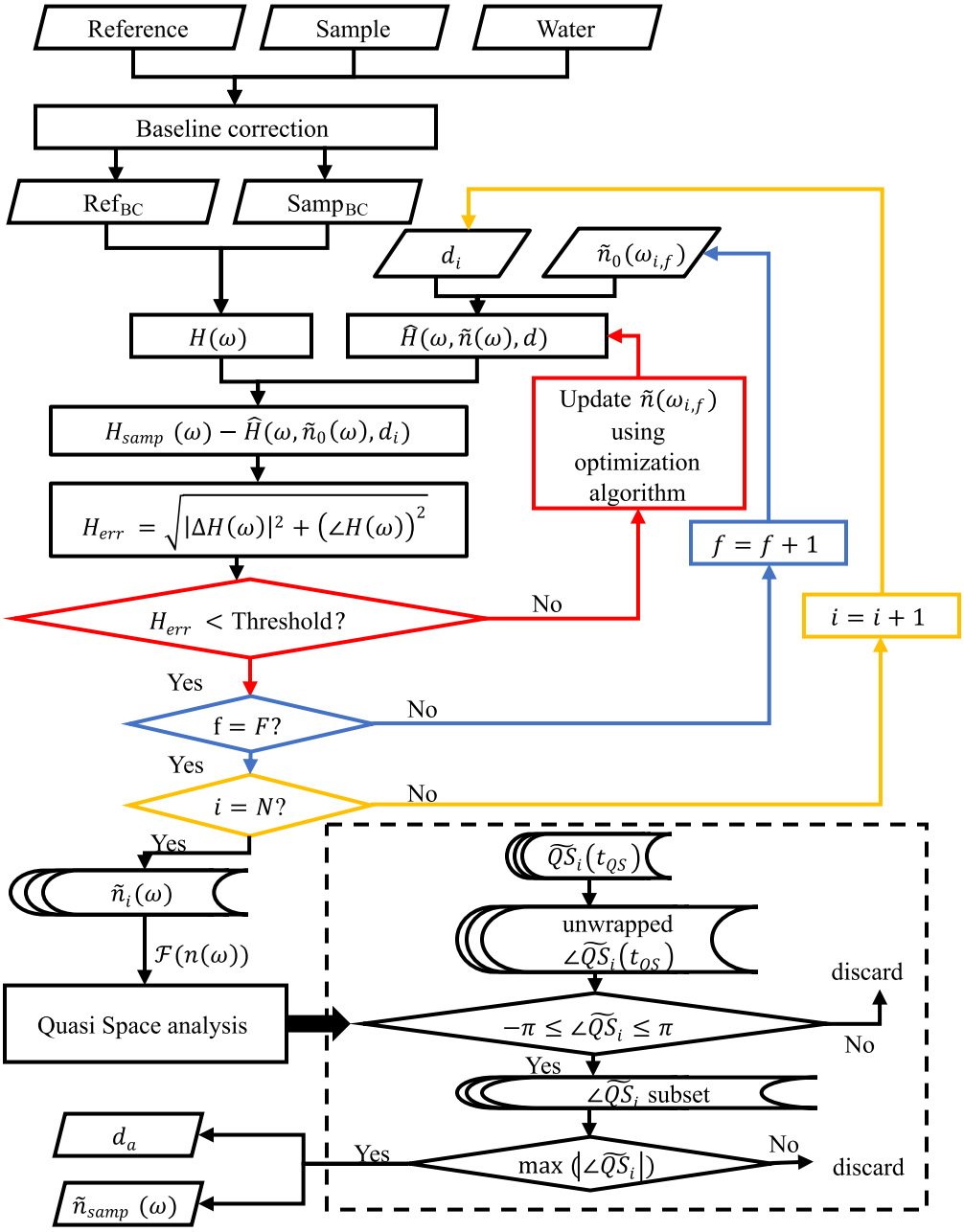

Fig. 6. The flow chart describes the process of simultaneously extracting the index of refraction and thickness of the air gap. An index of refraction is calculated for each thickness guess, d_N. An additional Fourier transform is applied to the set of refractive indices, and the extraction is completed in the quasi-space domain.

of all pixels are displayed in Fig. 7. Although the values do not fully agree with the expected value of 280μm, Fig. 7d suggests that the HDPE pellet was not flat, producing a variable air gap distance across its diameter.

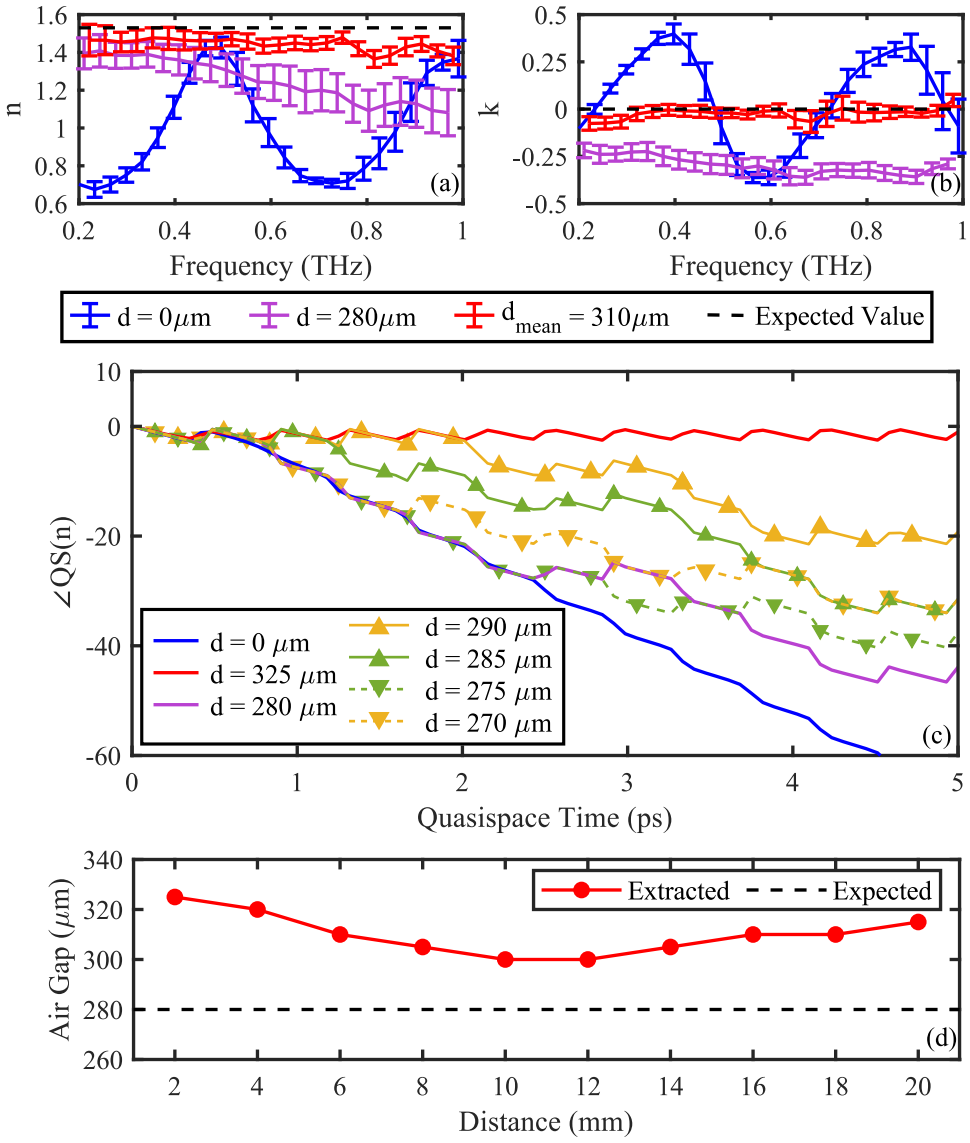

Fig. 7. The real (a) and imaginary (b) parts of the index of refraction of the HDPE pellet was extracted in three scenarios: assuming perfect contact between the sample and imaging window (blue trace), fixing the air gap to 280 μm (purple trace), and optimizing the depth of the void (red trace). The expected value of $\tilde{n} = 1.53 + j0$ is plotted for comparison. (c) The quasi-space domain phase of a representative pixel is shown. The quasi-space phase of the extracted thickness value is bound between $\pm\pi$. (d) The extracted thickness of the air gap across the sample was extracted, suggesting that the HDPE pellet does not have a uniformly flat surface.

5. Discussion

In many applications, THz-TDS measurements of multi-layered samples are desirable. These targets are susceptible to the formation of air gaps. Large voids present themselves as multiple peaks or valleys in the time-domain pulse. This characteristic is used to detect delaminations [35]

and varying thickness between paint layers in automobiles [36–38], monitor thickness and drying of paint [39], determine the quality of plastic welds [40], and art conservation [41, 42]. However, these applications require distinct pulses that can be isolated in the time domain. The time difference between the reflections is used to calculate the layer thickness. As demonstrated in Fig. 3a, an air gap of approximately hundred μm thickness does not produce separate THz pulses. Rather, the superposition of multiple reflections results in a single signal (black, solid trace) with an amplitude that is larger than what is expected (blue, dotted trace). Reconstructing the pulse in the time-domain provides an alternative method of extracting layer thicknesses, as illustrated by Fig. 3b. The proposed air gap model significantly improves the characterization of samples in non-ideal conditions. Following the flowchart presented in Fig. 4a, we are able to extract the index of refraction of the sample in the frequency-domain, as illustrated in Figs. 4b and c. However, this method is limited to producing single-layer topographic maps, such as Fig. 3, rather than multilayer B-scan images [38]. Additionally, the index of refraction may not be known *a priori* nor will the assumption of uniformity always hold true. Therefore, there is also a need for a method to simultaneously extract the refractive index of the sample and the thickness of the air gap. The quasi-space domain method is a more objective approach to characterizing a multi-layer sample structure.

We explored the effect of the imaginary part of the index of refraction (a lossy sample) on the results obtained by this method. Figure 8 demonstrates the simulated index of refraction of HDPE (low attenuation) and water (as an example of a material with high THz attenuation) [43] extracted at various $\Delta d = d - d_i$. The red trace represents the refractive index extracted at the correct thickness. Solid lines are values extracted at $\Delta d < 0$, while the dashed traces correspond to $\Delta d > 0$. The simulation presented in Figs. 8a and b reveals that the phase of the index of refraction of HDPE is reflected at the correct thickness in the real part and mirrored in the imaginary part. This is an alternative method to simultaneously extract the index of refraction and thickness of the air gap. However, this is only applicable to non-dispersive samples. This feature, however, as demonstrated in Figs. 8d and e is not observed in the case of water. Importantly though, as evident in Figs. 8c and f, in both scenarios the correct thickness produces the quasi-space domain phase with the largest amplitude of oscillation. Therefore, the quasi-space domain analysis is a more reliable and robust method of characterizing the sample and air gap, regardless of the sample's frequency-dependent behavior.

Finally, it should be noted that a fundamental resolution limit of our proposed approach is the useful bandwidth of the THz-TDS system. This is because at least one full Fabry-Peort oscillation cycle should be captured in the quasi-space domain for the associated air gap to be detected. Here, specially for the case of lossy samples, this bandwidth was often around 1 THz. For smaller air gaps, a larger bandwidth is needed, which can be possibly achieved by a combination of plasma-based THz sources and alternative detectors to PCAs [44].

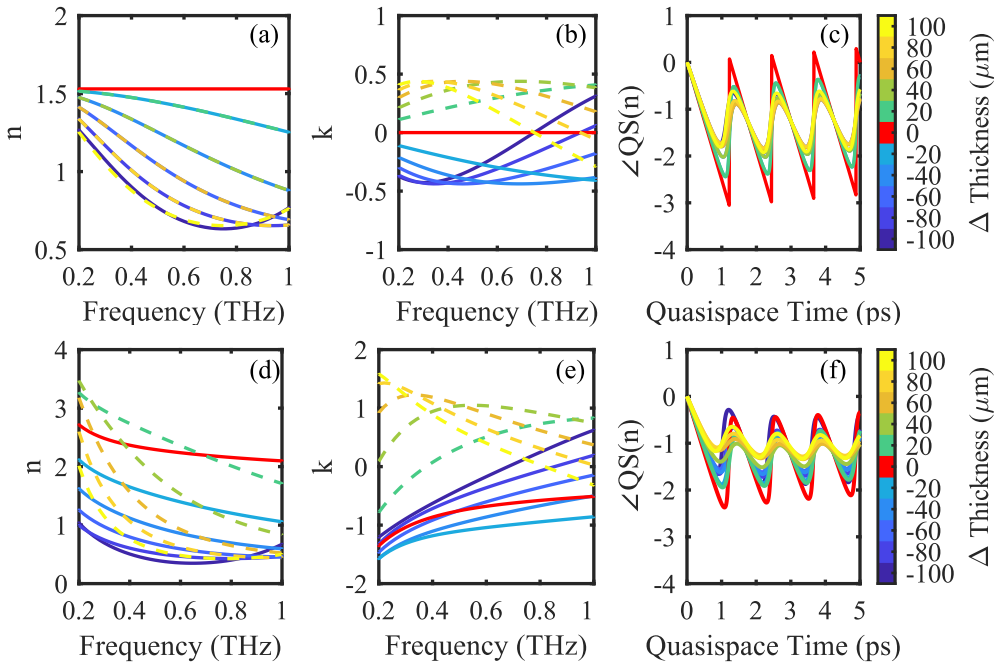

Fig. 8. The real and imaginary parts of the refractive indices of simulated (a,b) HDPE and (d,e) Water were extracted at different air gap thicknesses. The simulation reveals an alternative method of extracting the correct refractive index and thickness of the air gap (red lines). For non-dispersive materials such as HDPE, the correct thickness serves as a reflection and mirroring point in the real and imaginary parts of the index of refraction, respectively. This characteristic can not be applied to achromatic materials, such as water. The quasi-space technique is applicable to both samples and a more reliable method of extracting the thickness of the air gap, as demonstrated in (c) and (f).

6. Conclusion

We have described some of the spectral characteristics of a reflected THz-TDS signal affected by the presence of the air gap trapped between sample layers. We presented a multi-layer reflection transfer function that includes the propagation of the pulses through a hypothetically trapped air gap. This method was validated through two set of measurements and simulations. First, in a biological sample (skin burns), we were able to identify an air gap, extract the thickness in the time domain, and calculate the index of refraction of the skin in the frequency domain. Second, In a fabricated test sample of HDPE with an intentional air gap, we simultaneously extracted the thickness of the void and the index of refraction of the sample using a novel quasi-space phase analysis. We discussed the limitations of both methods, and proposed alternative approaches for extraction of air gap thickness. The methods presented in this paper can find potential use in improving measurements requiring an imaging window, quality control of automobile paint, and detection of delamination in non-destructive testing applications.

Funding. This work was supported in part by the U.S. Army Medical Research Acquisition Activity (USAMRAA) through the Military Burn Research Program (MBRP) under Award No. W81XWH-21-1-0258, the National Institute of General Medical Sciences (GM112693), and Stony Brook University.

Disclosures. MHA discloses intellectual property owned by the University of Washington, US Patent No. US9295402B1 [45].

Data availability. Data underlying the results presented in this paper are not publicly available at this time but may be obtained from the authors upon reasonable request.

References

1. A. Leitenstorfer, A. S. Moskalenko, T. Kampfrath, J. Kono, E. Castro-Camus, K. Peng, N. Qureshi, D. Turchinovich, K. Tanaka, A. G. Markelz, M. Havenith, C. Hough, H. J. Joyce, W. J. Padilla, B. Zhou, K.-Y. Kim, X.-C. Zhang, P. U. Jepsen, S. S. Dhillon, M. S. Vitiello, E. H. Linfield, A. G. Davies, M. C. Hoffmann, R. Lewis, M. Tonouchi, P. Klarskov, T. S. Seifert, Y. A. Gerasimenko, D. Mihailovic, R. Huber, J. L. Boland, O. Mitrofanov, P. Dean, B. Ellison, P. G. Huggard, S. P. Rea, C. P. Walker, D. T. Leisawitz, J. Gao, C. Li, Q. Chen, G. Valušis, V. P. Wallace, E. Pickwell-MacPherson, X. Shang, J. L. Hesler, N. M. Ridler, C. C. Renaud, I. Kallfass, T. Nagatsuma, J. A. Zeitler, D. A. Arnone, M. B. Johnston, and J. Cunningham, "The 2023 terahertz science and technology roadmap," J. Phys. D: Appl. Phys. **56**, 223001 (2023).
2. P. Jepsen, D. Cooke, and M. Koch, "Terahertz spectroscopy and imaging – modern techniques and applications," Laser & Photonics Rev. **5**, 124–166 (2011).
3. S. Y. Huang, Y. X. J. Wang, D. K. W. Yeung, A. T. Ahuja, Y. T. Zhang, and E. Pickwell-MacPherson, "Tissue characterization using terahertz pulsed imaging in reflection geometry," Phys. Med. Biol. **54**, 149 (2008).
4. H. Lindley-Hatcher, R. I. Stantchev, X. Chen, A. I. Hernandez-Serrano, J. Hardwicke, and E. Pickwell-MacPherson, "Real time THz imaging—opportunities and challenges for skin cancer detection," Appl. Phys. Lett. **118**, 230501 (2021).
5. G. G. Hernandez-Cardoso, L. F. Amador-Medina, G. Gutierrez-Torres, E. S. Reyes-Reyes, C. A. Benavides Martínez, C. Cardona Espinoza, J. Arce Cruz, I. Salas-Gutierrez, B. O. Murillo-Ortíz, and E. Castro-Camus, "Terahertz imaging demonstrates its diagnostic potential and reveals a relationship between cutaneous dehydration and neuropathy for diabetic foot syndrome patients," Sci. Rep. **12**, 1–10 (2022).
6. M. H. Arbab, T. C. Dickey, D. P. Winebrenner, A. Chen, M. B. Klein, and P. D. Mourad, "Terahertz reflectometry of burn wounds in a rat model," Biomed. optics express **2**, 2339–2347 (2011).
7. M. H. Arbab, T. C. Dickey, D. P. Winebrenner, A. Chen, and P. D. Mourad, "Characterization of burn injuries using terahertz time-domain spectroscopy," in *Advanced Biomedical and Clinical Diagnostic Systems IX,* vol. 7890 A. Mahadevan-Jansen, T. Vo-Dinh, and W. S. G. M.D., eds., International Society for Optics and Photonics (SPIE, 2011), p. 78900Q.
8. M. E. Khani, O. B. Osman, Z. B. Harris, A. Chen, J.-W. Zhou, A. J. Singer, and M. H. Arbab, "Accurate and early prediction of the wound healing outcome of burn injuries using the wavelet Shannon entropy of terahertz time-domain waveforms," J. Biomed. Opt. **27**, 116001 (2022).
9. M. E. Khani, Z. B. Harris, O. B. Osman, A. J. Singer, and M. H. Arbab, "Triage of in vivo burn injuries and prediction of wound healing outcome using neural networks and modeling of the terahertz permittivity based on the double debye dielectric parameters," Biomed. Opt. Express **14**, 918–931 (2023).
10. Z. D. Taylor, J. Garritano, S. Sung, N. Bajwa, D. B. Bennett, B. Nowroozi, P. Tewari, J. W. Sayre, J.-P. Hubschman, S. X. Deng, E. R. Brown, and W. S. Grundfest, "Thz and mm-wave sensing of corneal tissue water content: In vivo sensing and imaging results," IEEE Transactions on Terahertz Sci. Technol. **5**, 184–196 (2015).
11. A. Chen, Z. B. Harris, A. Virk, A. Abazari, K. Varadaraj, R. Honkanen, and M. H. Arbab, "Assessing corneal endothelial damage using terahertz time-domain spectroscopy and support vector machines," Sensors **22** (2022).
12. J. W. Zhou and M. H. Arbab, "Effective Debye relaxation models for binary solutions of polar liquids in the terahertz frequencies," Phys. Chem. Chem. Phys. (2021). Publisher: The Royal Society of Chemistry.
13. R. Koalla, N. Periketi, C. Ghorui, S. Mangali, and A. Chaudhary, "Terahertz time-domain spectroscopy, imaging and density functional theory based studies of 3, 4, 5 trinitro 1 h pyrazole," J. Mol. Struct. **1265**, 133449 (2022).
14. Y. Shen, a. T. Lo, P. Taday, B. Cole, W. Tribe, and M. Kemp, "Detection and identification of explosives using terahertz pulsed spectroscopic imaging," Appl. physics letters **86**, 241116 (2005).
15. M. E. Khani, Z. B. Harris, M. Liu, and M. H. Arbab, "Multiresolution spectrally-encoded terahertz reflection imaging through a highly diffusive cloak," Opt. Express **30**, 31550–31566 (2022).
16. K. Kawase, Y. Ogawa, Y. Watanabe, and H. Inoue, "Non-destructive terahertz imaging of illicit drugs using spectral fingerprints," Opt. express **11**, 2549–2554 (2003).
17. J. F. Federici, B. Schulkin, F. Huang, D. Gary, R. Barat, F. Oliveira, and D. Zimdars, "Thz imaging and sensing for security applications—explosives, weapons and drugs," Semicond. Sci. Technol. **20**, S266 (2005).
18. G. P. Kniffin and L. M. Zurk, "Model-based material parameter estimation for terahertz reflection spectroscopy," IEEE Transactions on Terahertz Sci. Technol. **2**, 231–241 (2012).
19. F. Vandrevala and E. Einarsson, "Decoupling substrate thickness and refractive index measurement in thz time-domain spectroscopy," Opt. Express **26**, 1697–1702 (2018).
20. L. Thrane, R. H. Jacobsen, P. U. Jepsen, and S. R. Keiding, "THz reflection spectroscopy of liquid water," Chem. Phys. Lett. **240**, 330–333 (1995).
21. P. U. Jepsen, U. Moller, and H. Merbold, "Investigation of aqueous alcohol and sugar solutions with reflection terahertz time-domain spectroscopy," Opt. Express **15**, 14717–37 (2007).
22. P. C. Ashworth, E. Pickwell-MacPherson, E. Provenzano, S. E. Pinder, A. D. Purushotham, M. Pepper, and V. P. Wallace, "Terahertz pulsed spectroscopy of freshly excised human breast cancer," Opt. express **17**, 12444–12454 (2009).

23. Q. Sun, E. P. Parrott, Y. He, and E. Pickwell-MacPherson, "In vivo thz imaging of human skin: Accounting for occlusion effects," J. biophotonics **11**, e201700111 (2018).
24. T. D. Dorney, R. G. Baraniuk, and D. M. Mittleman, "Material parameter estimation with terahertz time-domain spectroscopy," JOSA A **18**, 1562–1571 (2001).
25. M. Scheller, C. Jansen, and M. Koch, "Analyzing sub-100-μm samples with transmission terahertz time domain spectroscopy," Opt. Commun. **282**, 1304–1306 (2009).
26. I. Pupeza, R. Wilk, and M. Koch, "Highly accurate optical material parameter determination with thz time-domain spectroscopy," Opt. express **15**, 4335–4350 (2007).
27. M. H. Arbab, A. Chen, E. I. Thorsos, D. P. Winebrenner, and L. M. Zurk, "Effect of surface scattering on terahertz time domain spectroscopy of chemicals," in *Terahertz Technology and Applications,* vol. 6893 K. J. Linden and L. P. Sadwick, eds., International Society for Optics and Photonics (SPIE, 2008), p. 68930C.
28. M. H. Arbab, D. P. Winebrenner, E. I. Thorsos, and A. Chen, "Application of wavelet transforms in terahertz spectroscopy of rough surface targets," in *Terahertz Technology and Applications III,* vol. 7601 L. P. Sadwick and C. M. M. O'Sullivan, eds., International Society for Optics and Photonics (SPIE, 2010), p. 760106.
29. M. Ebrahimkhani and M. H. Arbab, "Extraction of thz absorption signatures obscured by rough surface scattering using discrete wavelet transform," in *2018 43rd International Conference on Infrared, Millimeter, and Terahertz Waves (IRMMW-THz),* (2018), pp. 1–2.
30. S. Huang, P. C. Ashworth, K. W. Kan, Y. Chen, V. P. Wallace, Y.-t. Zhang, and E. Pickwell-MacPherson, "Improved sample characterization in terahertz reflection imaging and spectroscopy," Opt. Express **17**, 3848–3854 (2009).
31. O. Osman, Z. Harris, J. Zhou, M. Khani, A. Singer, and M. Arbab, "In vivo assessment of burn depth and wound healing using a handheld terahertz hyperspectral scanner," Adv. Photonics Res. p. 2100095 (2022).
32. A. J. Singer, J. W. Zhou, O. B. Osman, Z. B. Harris, M. E. Khani, E. Baer, N. Zhang, S. A. McClain, and M. H. Arbab, "Comparison of comparable scald and contact burns in a porcine model: A preliminary report," Wound Rep Reg. **28**, 789–796 (2020).
33. Z. B. Harris and M. H. Arbab, "Terahertz phasr scanner with 2 khz, 100 ps time-domain trace acquisition rate and an extended field-of-view based on a heliostat design," IEEE Transactions on Terahertz Sci. Technol. **12**, 619–632 (2022).
34. O. B. Osman, Z. B. Harris, M. E. Khani, J. W. Zhou, A. Chen, A. J. Singer, and M. H. Arbab, "Deep neural network classification of in vivo burn injuries with different etiologies using terahertz time-domain spectral imaging," Biomed. Opt. Express **13**, 1855–1868 (2022).
35. J. F. Federici, D. Gary, R. Barat, and D. Zimdars, "Thz standoff detection and imaging of explosives and weapons," in *Optics and Photonics in Global Homeland Security,* vol. 5781 (International Society for Optics and Photonics, 2005), pp. 75–84.
36. J. Dong, A. Locquet, M. Melis, and D. Citrin, "Global mapping of stratigraphy of an old-master painting using sparsity-based terahertz reflectometry," Sci. reports **7**, 1–12 (2017).
37. T. Yasuda, T. Iwata, T. Araki, and T. Yasui, "Improvement of minimum paint film thickness for thz paint meters by multiple-regression analysis," Appl. optics **46**, 7518–7526 (2007).
38. K. Su, Y.-C. Shen, and J. A. Zeitler, "Terahertz sensor for non-contact thickness and quality measurement of automobile paints of varying complexity," IEEE Transactions on Terahertz Sci. Technol. **4**, 432–439 (2014).
39. T. Yasui, T. Yasuda, K.-i. Sawanaka, and T. Araki, "Terahertz paintmeter for noncontact monitoring of thickness and drying progress in paint film," Appl. Opt. **44**, 6849–6856 (2005).
40. S. Wietzke, C. Jördens, N. Krumbholz, B. Baudrit, M. Bastian, and M. Koch, "Terahertz imaging: a new non-destructive technique for the quality control of plastic weld joints," J. Eur. Opt. Soc. Publ. **2** (2007).
41. J. Jackson, M. Mourou, J. Whitaker, I. Duling Iii, S. Williamson, M. Menu, and G. Mourou, "Terahertz imaging for non-destructive evaluation of mural paintings," Opt. communications **281**, 527–532 (2008).
42. J. Dong, J. B. Jackson, M. Melis, D. Giovanacci, G. C. Walker, A. Locquet, J. W. Bowen, and D. Citrin, "Terahertz frequency-wavelet domain deconvolution for stratigraphic and subsurface investigation of art painting," Opt. express **24**, 26972–26985 (2016).
43. J. T. Kindt and C. A. Schmuttenmaer, "Far-infrared dielectric properties of polar liquids probed by femtosecond terahertz pulse spectroscopy," J. Phys. Chem. **100**, 10373–10379 (1996).
44. K. Xu, M. Liu, and M. H. Arbab, "Broadband terahertz time-domain polarimetry based on air plasma filament emissions and spinning electro-optic sampling in gap," Appl. Phys. Lett. **120** (2022).
45. M. H. Arbab, P. D. Mourad, A. Chen, T. C. Dickey, M. D. Klein, and D. P. Winebrenner, "Methods and systems for assessing a burn injury," (2016). US Patent 9,295,402.